Available online at www.sciencedirect.com
SCIENCE DIRECT®
Journal of Nuclear Materials 346 (2005) 266–271
journal of nuclear materials
www.elsevier.com/locate/jnucmat

Electrostatic dust detection on remote surfaces

C. Voinier [a], C.H. Skinner [b,*], A.L. Roquemore [b]

[a] The College of New Jersey, Ewing, NJ 08628, USA
[b] Princeton Plasma Physics Laboratory, Princeton University, Princeton, NJ 08543, USA

Received 3 March 2005; accepted 24 June 2005

Abstract

The inventory of dust in next-step magnetic fusion devices will be regulated for safety reasons, however diagnostics to measure in-vessel dust are still in their infancy. Advances in dust particle detection on remote surfaces are reported. Grids of interlocking circuit traces with spacing in the range 125–25 μm were biased to 30 V. Impinging dust creates a short circuit and the resulting current pulse was recorded. The detector response was measured with particles scraped from a carbon fiber composite tile and sorted by size category. The finest 25 μm grid showed a sensitivity more than an order of magnitude higher than the 125 μm grid. The response to the finest particle categories (5–30 μm) was two orders of magnitude higher than the largest (125–250 μm) category. Longer duration current pulses were observed from the coarser particles. The results indicate a detection threshold for fine particles below 1 μg/cm^2.
© 2005 Elsevier B.V. All rights reserved.

PACS: 52.40.Hf; 52.90.+z

1. Introduction

Dust particles are ubiquitous on interior surfaces of current tokamaks [1–6] though dust particle production has not been observed directly. Recent calculations have highlighted the mobility of dust particles in the electric and magnetic fields of a tokamak and the possibility of plasma contamination from mobile dust [7]. The more intense plasma surface interactions and longer pulse duration in next-step devices such as ITER is expected to lead to much higher accumulations of dust [8]. These dust particles will be radioactive from tritium or activated metals, toxic and/or chemically active with steam or air and the inventory of dust will be strictly limited to avoid adverse safety consequences. Proposed limits are 10–20 kg of beryllium dust on hot surfaces, 100 kg for carbon dust, and 100–400 kg for tungsten dust (depending on the containment function of the ITER building) [9]. However diagnostics to remotely measure dust inventories in a next-step machine and assure compliance with safety limits have not yet been demonstrated. Measuring dust particle inventories is a challenge in existing machines, let alone one with the complexity and radiological environment of ITER [10–12]. However measured, once the dust inventory in ITER approaches the safety limit, dust removal will be necessary to enable continued plasma operations. Removal techniques, however, are also in their infancy.

A novel device to detect dust particles that have settled on a remote surface has recently been developed in the laboratory [13,14]. Two closely interlocking grids of

* Corresponding author. Tel.: +1 609 243 2214; fax: +1 609 243 2265.
E-mail address: cskinner@pppl.gov (C.H. Skinner).

0022-3115/$ - see front matter © 2005 Elsevier B.V. All rights reserved.
doi:10.1016/j.jnucmat.2005.06.018

conductive traces on a circuit board were biased to 30–50 V. Test particles, scraped from a carbon fiber composite tile, were delivered to the grid by a stream of nitrogen. Miniature sparks appeared when the particles landed on the energized grid and created a transient short circuit. Typically the particles vaporized in a few seconds restoring the previous voltage standoff. The transient current flowing through the short circuit created a voltage pulse that was recorded by standard nuclear counting electronics. The device worked well in both at atmosphere and in vacuum environments. Because of its electrostatic operating principle, this device does not provide an absolute measure of the mass of dust – such a diagnostic still needs to be developed for a tokamak environment. However the tests showed a clear correlation between the recorded counts and particle concentration, especially at finer grid spacings.

In the previous work carbon particles of a scale 1–500 μm were used with most of the particles being in the smaller size range. Grids of spacing 127–762 μm were tested. In the present work, grids of extra fine (25 μm) spacing were used. The closer match of grid spacing to the size of the majority of particles resulted in greatly enhanced response. In the previous work the particles had a wide range in size and it was not clear whether large or small particles, or both, cause the dominant response. To address this issue, test particles were sorted by size using sieves of 5–250 μm pore size and the response and sensitivity of the detector to the particles as a function of particle size was measured.

2. Experimental setup

The experimental method followed the technique of Ref. [13]. A 2.5 cm i.d. pipe with a 90° bend was used to deliver a controlled amount of particles to the grid in a stream of nitrogen gas. In the present work the geometry was modified slightly. The vertical section of pipe was 2.3 cm long (cf. 18 cm used in Ref. [13]) and the distance between the pipe and grid was 5 cm (cf. 6 cm in Ref. [13]). The distance between the particle delivery port and the nitrogen supply was shortened from 3 cm to 1.3 cm. A known amount of particles was introduced to the delivery tube and a continuous flow of nitrogen carried the particles to grid which was biased at 30 V. The impinging particles created a short circuit and the particles were vaporized, often with a visible spark. The resulting current pulse flowed through a 51 Ω resistor creating an irregular voltage pulse that was filtered by a band pass filter (1.3–31 kHz) and input to a single channel analyzer that produced an output pulse when the signal decreased past 0.4 V. After 10 s the nitrogen flow was turned off and the number of pulses counted by the electronics was recorded. After each measurement the delivery tube, grid and surrounding area were cleaned with compressed gas.

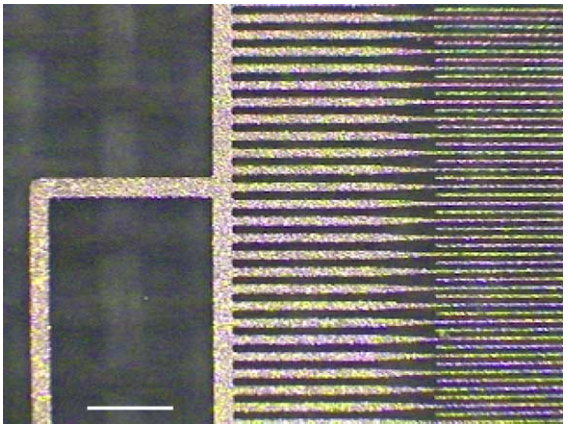

Fig. 1. Partial view of circuit grid showing the branching to the finely spaced traces interspersed with the corresponding traces from the right hand side. In the active region the width of the trace is 25 μm and the trace spacing is 25 μm. The scale bar corresponds to 500 μm.

For the present work we were able to obtain finer grids than used previously, with spacing down to 25 μm (Fig. 1). The substrate was woven glass reinforced polytetrafluorethylene (PTFE) microwave laminate substrate (Ultralam 2000) that is classified by NASA as a low outgassing material. A seed layer of 100 nm of titanium and copper was sputtered onto the material, followed by electroplating with a 2 μm layer of copper and then the interlocking grid pattern was etched by photolithography. The traces were the same width as the spacings and the active area of the grid was 1.2×1.2 cm. In the absence of dust, the 25 μm grid was able to stand off a voltage up to 240 V, much higher than the operating ranging of 30 V.

3. Sifting the dust by size

Fig. 2 shows images of the particles as scraped from the carbon fiber composite tile taken with a digital optical microscope. The particles were irregular in shape, and included a few fibers. The particles were sorted into different size classes by sifting through a sequence of vibrating sieves in an Allen–Bradley sonic sifter model L3PF. The sieves were vibrated continuously with a periodic knocking to breakup any clumps of particles. In addition the sieves were manually rotated every 3 min and the sides lightly tapped every 15 min in order to break up clumps and release any particles attached to the side support of a sieve. The dimensions of the apertures in the 250 μm, 125 μm, 53 μm and 30 μm sieves were checked with the digital microscope. The length of the side of the square aperture showed some variation

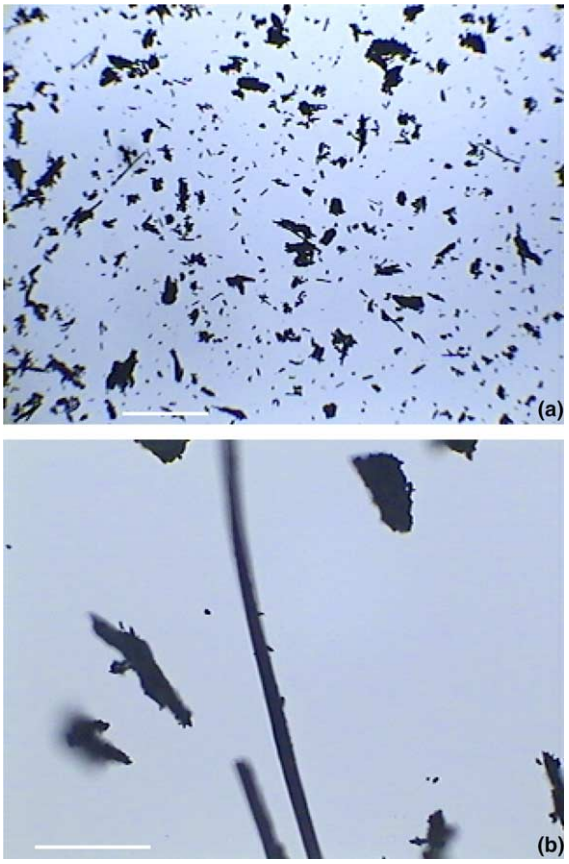

Fig. 2. (a) Image of unsifted dust, the scale bar corresponds to 500 μm. (b) Image of dust showing a long fiber. The scale bar corresponds to 50 μm.

from aperture to aperture but was within 20% of the nominal value. The size of the 20 μm and 5 μm sieves is stated by the manufacturer to be within ±2 μm of the nominal value.

The sifting was done in two stages. First the particles were sifted for 30 min through a stack of three sieves of 30 μm, 20 μm and 5 μm with the coarsest sieve on top. Very few particles were transmitted through the 5 μm sieve, possibly because they were electrostatically attached to larger particles. Particles remaining on the 30 μm sieve were then sifted again for 30 min through a stack of 250 μm, 125 μm and 53 μm sieves. The particle categories are labeled by filter size, i.e., 53–125 μm particles were transmitted through the 125 μm filter but retained by the 53 μm filter.

To characterize the size distribution of the sifted and unsifted particles a sample was gently blown with a hand puffer onto a clean glass slide and viewed in the digital microscope. A 40× objective (image size 251 × 337 μm, pixel size 1 μm) was used for particles sifted through sieves of ⩽125 μm and for the unsifted particles. A 10× objective (image size 1004 × 1348 μm, pixel size 4 μm) was used for larger particles that did not pass through the 125 μm sieve. Several digital images for each particle

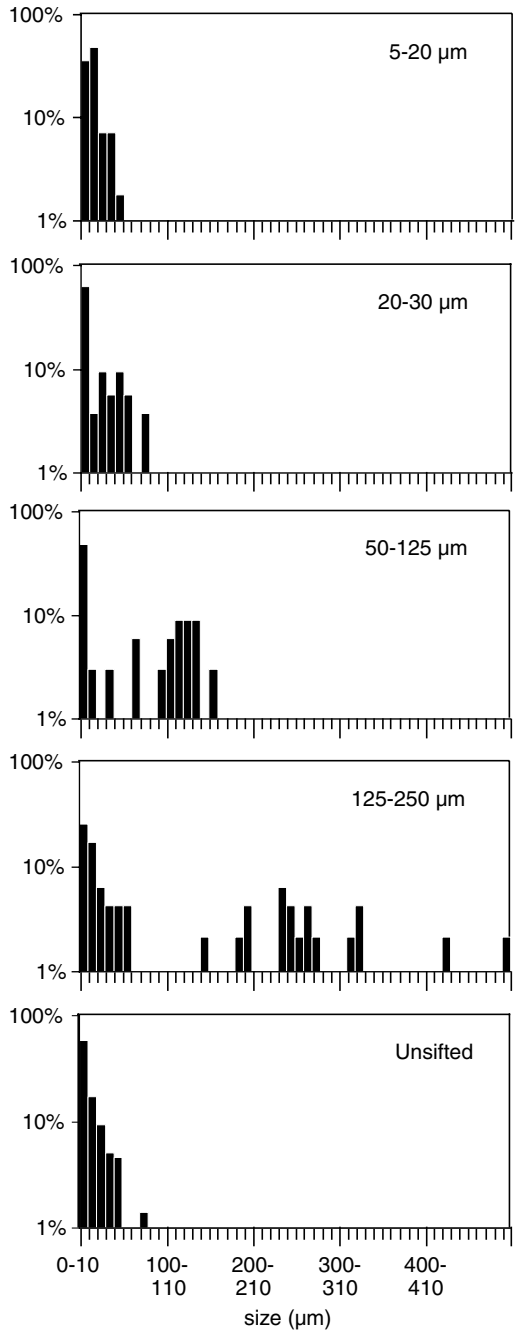

Fig. 3. Particle size distribution before and after sifting. The size is the projected area diameter as defined by Eq. (1). The number of particles in each category is normalized to 100%. The larger number in the legend indicates the filter that transmitted the particles and the lower number the filter that retained the particles.

category were combined into montages and analyzed using ImageJ [15] software. This converted the gray-scale image into black and white and listed the area of each particle. A montage of 2×2 images was used for the 5–20 μm and 20–30 μm particle categories while a montage of 4×4 images was used for the 53–125 μm, 125–250 μm and the unsifted particle categories. The projected area diameter, D_{PA}, (diameter of a spherical particle with equivalent area) was derived from the area measured by ImageJ, using: [16]

$$D_{PA} = 2 \times \sqrt{\frac{\text{Area}}{\pi}} \quad (1)$$

The normalized size distributions are shown in Fig. 3. The size of the unsifted particles are predominantly $D_{PA} < 20$ μm. While some fine particles remain behind on the filters, the population of particles with $D_{PA} > 20$ μm is greatly enhanced in the larger size categories by the sifting process.

The particle delivery efficiency was measured by substituting a collection bin for the grid and weighing both the dust supplied and that delivered to the collection bin. The amount of particles used was generally larger than that used in the subsequent experiments with the grid in order to improve the measurement accuracy. The delivery efficiency was measured for all the particle size categories and is shown in Fig. 4. There was a significant scatter in the data, as observed in the previous work, however the efficiency for the finer particles appeared to be somewhat lower than the larger and unsifted particles, possibly due to clumping of the fine particles. The delivery efficiency, E, and regression coefficient, R^2 from a linear fit to the data is shown in Table 1. This data is used to estimate the areal density of particles incident on the grid.

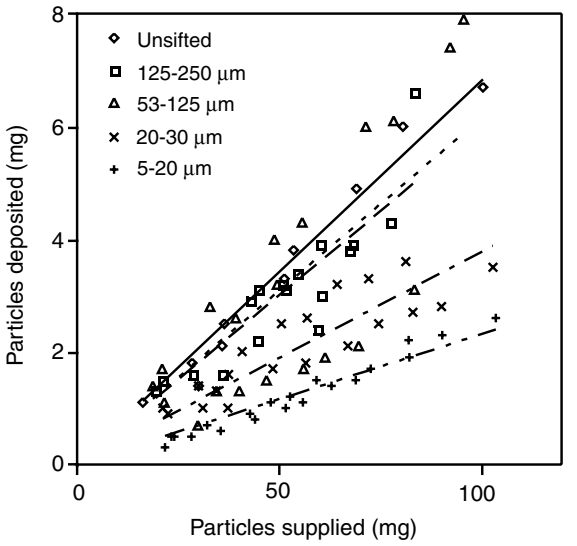

Fig. 4. Delivery efficiency for different size categories of particles. The lines are linear fits to the data (see Table 1). The delivery efficiency is systematically lower for the smaller particle categories.

Table 1
Delivery efficiency of various particle categories

Category	Efficiency (%)	R^2
Unsifted	6.8	0.97
125–250 μm	6	0.79
53–125 μm	6.1	0.61
20–30 μm	3.7	0.77
5–20 μm	2.3	0.94

4. Results

Fig. 5 shows the electrical signals resulting from particles incident on a 125 μm spaced grid with tin coated traces. The two upper traces show the signal before and after the (1.3–31 kHz) band pass filter and the lowest trace shows the pulses generated by the single channel analyser when the filtered signal crossed 0.4 V in a negative direction. The filtered signals for 5–20 μm category particles (upper panel) have a duration of order 1 μs, while much longer duration ≈30 μs pulses can occur with the larger category 125–250 μm particles. The longer 'burn-up' time appears to be due to the larger particles present in this category. So, in addition to counting events due to particles impinging on the grid, this detector can also yield information on the size of the particles from the electrical waveforms.

A dramatic increase in sensitivity was observed for the finer grids. Grids of spacing of 127 μm, 102 μm, 76 μm, 51 μm, and 25 μm were tested with unsifted dust and the results are shown in Fig. 6. The number of counts recorded for a given concentration of dust increased by more than an order-of-magnitude with the finest 25 μm spacing grid. The response is slightly higher than linear, an indication that some particles link up to form a 'bridge' between the traces at higher concentrations.

In the unsifted particle category most of the particles have a projected area diameter below 10 μm (Fig. 3) however there are a few long fibers. Particles impinging on the grid bridge the gap between the traces forming a short circuit. This could be done by one large fiber or by a chain of several fine particles. It is not clear from tests with unsifted particles whether the grid response is more from many fine particles or from single long fibers that can span the distance between the traces. To address this issue the 25 μm grid was tested with sifted particles and the results are shown in Fig. 7. For the same areal density (mg/cm^2) of particles impinging on the grid, the response from particles in the finest categories 5–20 μm and 20–30 μm was two orders-of-magnitude higher than

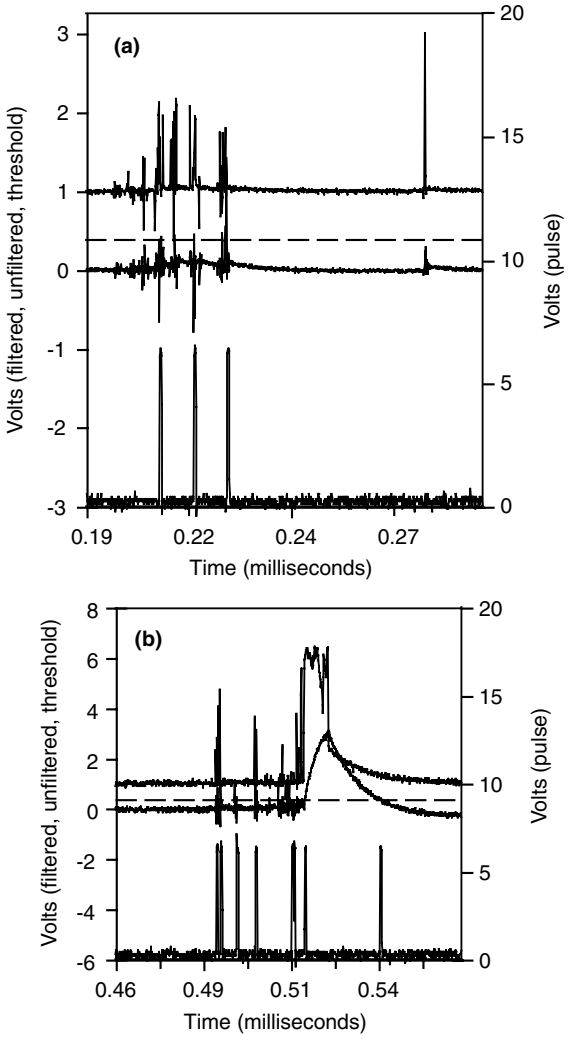

Fig. 5. The upper panel (a) was generated using the 5–20 μm particle category and the lower panel (b) from the 125–250 μm category with a 125 μm spaced grid with tin coated traces. In each panel the upper waveform is the voltage signal across the 51 Ω resistor arising from a short circuit, the middle waveform is the signal after a 1.3–31 kHz bandpass filter (y-axis on left), and the lower waveform the pulses output by the SCA (y-axis on right). It can be seen that the pulse duration could be significantly longer in the larger particle category.

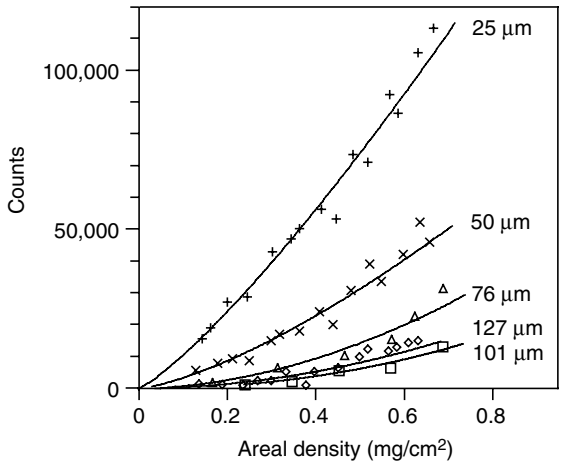

Fig. 6. Response of grids to unsifted particles showing an increase in counts for the finer grids by more than one order-of-magnitude. The grid spacing is listed on the right and is: (+) 25 μm; (×) 50 μm; (△) 76 μm; (□) 101 μm; (◇) 127 μm. The lines are a second order polynomial fit to the data.

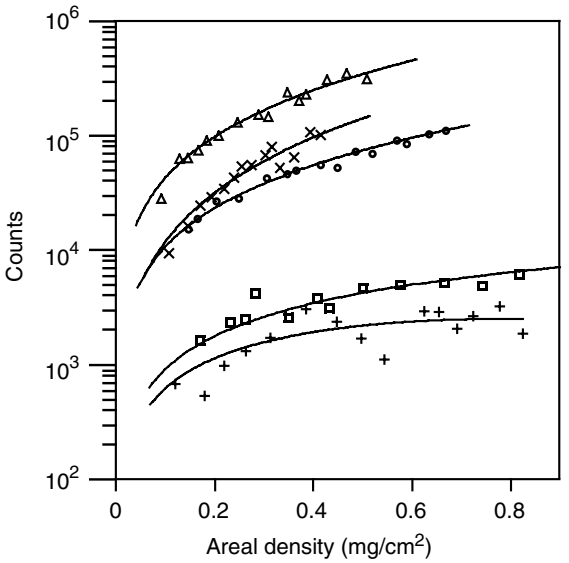

Fig. 7. Response of the 25 μm grid to sifted particles: (×) 5–20 μm; (△) 20–30 μm; (□) 53–125 μm; (+) 125–250 μm; (○) unsifted. The lines are a second order polynomial fit to the data.

for the coarse 125–250 μm category. The response to unsifted particles was almost as high as the fine sifted particles as expected because most of the unsifted particles are of 10 μm scale.

Of course there are many more particles in the fine category than in the same mass of particles in a coarse category so it appears that the number of incident particles is more a determining factor in the detector response than their areal density in mg/cm^2. The relative average mass of particles in each category may be estimated from the ImageJ analysis of the particle areas. The particle volume and hence mass is approximated by the area raised to the power 3/2. In this approximation, the relation between the number of counts and number of incident particles is close to linear, though there are clearly other factors at work as evidenced by the somewhat higher response to 20–30 μm particles than the 5–20 μm particles. Extrapolation of the above results to low particle densities indicates that the detection

threshold, defined as the areal density needed to generate 100 counts, is below 1 μg/cm^2 for the finest particle category.

5. Conclusions

The sensitivity of a novel detector for dust particles on remote surfaces has been enhanced by more than an order of magnitude by the use of ultrafine grids (25 μm spacing). The response to particles of different size categories was compared and the sensitivity, expressed in counts/areal density (mg/cm^2) of particles, was maximal for the finest particles. This is a favorable property for tokamak dust which is predominantly of micron scale. It appears that the number density of incident particles (whatever their size) is a dominant factor in the grid response. Qualitative information on the size of the particles is apparent in the current pulse created by the short circuit. This device shows promise for the detection of conductive dust settling in remote inaccessible areas in fusion devices. This device could also be applied to controlling the dust levels. Since dust particles are vaporized on contact with the grid, one could envisage a mosaic of these devices that would ensure that specific areas remained dust free. In the future nanoengineered traces on a low activation substrate such as SiO_2 could be applied to detect metallic or mixed material dust in an activated environment. Further development is in progress to test these possibilities.

Acknowledgements

The authors appreciate discussions with S. Zinkle, and thank D. LaBrie, T. Provost, and H. Schneider for technical assistance. C. Voinier acknowledges support from the 2004 National Undergraduate Fellowships in Plasma Physics and Fusion Energy Sciences. The ultrafine grids were supplied by MicroConnex of Snoqualmie, WA. This work was funded by US DOE Contract No. DE-AC02-76CH03073.

References

[1] W.J. Carmack, R.A. Anderl, R.J. Pawelko, G.R. Smollik, K.A. McCarthy, Fus. Eng. Des. 51-2 (2000) 477.
[2] J. Winter, Plasma Phys. Control Fus. 40 (1998) 1201.
[3] A.T. Peacock, P. Andrew, P. Cetier, J.P. Coad, G. Federici, F.H. Hurd, M.A. Pick, C.H. Wu, J. Nucl. Mater. 266–269 (1999) 423.
[4] Ph. Chappuis, E. Tsitrone, M. Mayne, X. Armand, H. Linke, H. Bolt, D. Petti, J.P. Sharpe, J. Nucl. Mater. 290–293 (2001) 245.
[5] M. Rubel, M. Cecconello, J.A. Malmberg, G. Sergienko, W. Biel, J.R. Drake, A. Hedqvist, A. Huber, V. Philipps, Nucl. Fus. 41 (2001) 1087.
[6] J.P. Sharpe, P.W. Humrickhouse, C.H. Skinner, T. Tanabe, K. Masaki, N. Miya, A. Sagara, J. Nucl. Mater. 337–339 (2005) 1000.
[7] S.I. Krasheninnikov, Y. Tomita, R.D. Smirnov, R.K. Janev, Phys. Plasmas 11 (2004) 3141.
[8] G. Federici, C.H. Skinner, J.N. Brooks, J.P. Coad, C. Grisolia, A.A. Haasz, A. Hassanein, V. Philipps, C.S. Pitcher, J. Roth, W.R. Wampler, D.G. Whyte, Nucl. Fus. 41 (2001) 1967.
[9] S.J. Piet, A. Costley, G. Federici, F. Heckendorn, R. Little, in: Proceedings of the 17th IEEE/NPSS Symposium on Fusion Engineering, San Diego, 6–10 October 1997, IEEE, Piscataway, NJ, USA, 1998, p. 321.
[10] G.F. Counsell, C.H. Wu, Phys. Scr. T91 (2001) 70.
[11] R. Reichle et al., J. Nucl. Mater. 290–293 (2001) 701.
[12] G.T. Razdobarin, G. Federici, V.M. Kozhevin, E.E. Mukhin, V.V. Semenov, S.Y. Tolstyakov, Fus. Sci. Technol. 41 (2002) 32.
[13] A. Bader, C.H. Skinner, A.L. Roquemore, S. Langish, Rev. Sci. Instrum. 75 (2004) 370.
[14] C.H. Skinner, A.L. Roquemore, A. Bader, W.R. Wampler, Rev. Sci. Instrum. 75 (2004) 4213.
[15] Available from: <http://rsbweb.nih.gov/ij/>.
[16] W.J. Carmack et al., Fus. Eng. Des. 39&40 (1998) 479.